Numerical analysis of rubber balloons

Erwan Verron, Gilles Marckmann

Numerical analysis of rubber balloons

E. Verron *, G. Marckmann

Laboratoire de Mécanique et Matériaux, Division Structures, École Centrale de Nantes, BP 92101, 44321 Nantes cedex 3, France

Abstract

The present paper deals with the inflation of two connected rubber balloons. This problem is known to exhibit instabilities and complex equilibrium paths. In some cases, the balloons inflate asymmetrically and equilibrium states with unequal radii take place. In this work, balloons are considered axisymmetric and discretized using an efficient B-spline discretization. The non-linear finite element procedure is associated with a stability and post-bifurcation analysis in order to determine singular points and to switch onto secondary equilibrium branches. The case of Mooney–Rivlin membranes is thoroughly investigated and the branching diagrams obtained are discussed in regards with the material parameters.

Keywords: Membrane inflation; Rubber balloons; Stability; Equilibrium paths

1. Introduction

The inflation of two connected rubber balloons was first examined by Miller [1]. He describes the simple experiment that consists of blowing two rubber balloons fixed on the ends of a T tube. Its motivation was to demonstrate that the balloons behave as soap bubbles for which the smaller blows up the larger one until the latter disappears [2,3]. He did not observe what he was expecting, but he did not describe what phenomenon he observed. Later Weinhaus and Barker [4] considered this problem and explained the difference between the soap bubbles and the balloons by invoking their highly different constitutive behaviours. They proposed a realistic

* Corresponding author. Tel.: +33-2-40-37-25-14; fax: +33-2-40-37-25-73.
E-mail address: erwan.verron@ec-nantes.fr (E. Verron).

solution by employing the neo-Hookean strain energy function for the balloons. They demonstrated that the final states of the two balloons often occur with unequal and non-zero radii if the amount of gas injected is sufficiently large. In a more recent paper, Read [5] used the generalised Hooke's law to model the behaviour of rubber under large strains and a similar analytical procedure to solve the problem. Müller and co-workers [6,7] considered the Mooney–Rivlin hyperelastic constitutive equation for rubber. They investigated the possible equilibria of the two balloons by modelling the thermodynamics of the global system, including the balloons and the inflating gas. They highlighted that even if some equilibria are involved with different radii, large strains equilibria with equal radii can take place for large amounts of inflating gas.

The present paper deals with the problem of interconnected toy balloons with the use of numerical methods. The system of two balloons is supposed to be initially and to remain axisymmetric during the inflation. The material obeys the Mooney–Rivlin strain energy and the influence of the material parameters is discussed in order to recover the different solutions mentioned above. In Section 2, the governing equations for the inflation of axially symmetric hyperelastic membrane and the stress-strain relationships are briefly recalled. The present approach is highly based on the work of Green and Adkins who first derived the equations of inflated membranes [8]. More bibliographical references on this subject can be found in Khayat et al. [9]. In order to solve these non-linear equations, the membrane is interpolated by B-spline finite elements and the corresponding discretized system is established in Section 3. In the same section, the numerical procedure is presented. The emphasise is laid on the treatment of singular points that is needed to explore the whole branching diagram, said to investigate bifurcating solutions in which unequal radii states take place. Section 4 is devoted to the numerical results. The behaviour of a single balloon is briefly recalled. The influence of the material parameters on the solution is highlighted. Then, the problem of connected balloons is thoroughly examined. The different equilibrium paths are computed depending on material parameters. Final remarks are given in Section 5.

2. Inflation of axially symmetric hyperelastic membranes

2.1. Kinematics

Consider a thin membrane which mid-surface is described by cylindrical co-ordinates (r_0,θ_0,z_0) in the undeformed stress-free state and (r,θ,z) in the deformed loaded state. The membrane is assumed z_0-axially symmetric, so that the position of a membrane particle can be described using only the arc-length co-ordinate s in both undeformed and deformed configurations. Thus, in each θ_0-constant plane, we have:

$$r_0 = r_0(s) \quad ; \quad z_0 = z_0(s) \tag{1}$$

and:

$$r = r(s) \;\; ; \;\; \theta = \theta_0 \;\; ; \;\; z = z(s) \tag{2}$$

In these equations, s varies from 0 to l_0, the initial length of the membrane cross-section. Moreover, the undeformed and deformed membrane thickness, respectively h_0 and h, are both functions of s. In the present work, the initial thickness is considered uniform along the cross-section.

Some basic kinematics relations are now recalled. In axially symmetric inflation problems, the principal directions of stretch are known at each particle of the membrane. They are meridian (indexed 1), circumferential (indexed 2) and normal (indexed 3) to the cross-section. The corresponding principal stretches are given by:

$$\lambda_1 = \sqrt{\frac{r'^2 + z'^2}{r'^2_0 + z'^2_0}} \;\; ; \;\; \lambda_2 = \frac{r}{r_0} \;\; ; \;\; \lambda_3 = \frac{h}{h_0} \tag{3}$$

where the notation—$'$stands for the differentiation with respect to s. Note that due to the material incompressibility, these stretches are related by:

$$\lambda_1\lambda_2\lambda_3 = 1 \tag{4}$$

In the context of membrane inflation, this relation is used to calculate the deformed thickness with the use of the two in-plane stretches λ_1 and λ_2:

$$h = \frac{h_0}{\lambda_1\lambda_2} \tag{5}$$

2.2. Constitutive equation

Non-linear elastic rubber-like materials are classically modelled by hyperelastic constitutive equations. Thus, the material behaviour is represented by a strain energy function per unit of volume, denoted w. The Cauchy stresses are then defined as the partial derivatives of the strain energy with respect to stretches [10]:

$$\sigma_i = \lambda_i w_i - q \qquad i = 1,2,3 \tag{6}$$

where w_i stands for the differentiation of w with respect to λ_i and q represents the hydrostatic pressure that ensures the incompressibility assumption. Due to this arbitrary parameter, only stress differences are explicitly defined. In the case of membranes, this difficulty is overcome by considering that the structure remains under plane stress conditions, said $\sigma_3 = 0$. Thus, the two in-plane Cauchy stresses are given by:

$$\sigma_1 = \lambda_1 w_1 \;\; ; \;\; \sigma_2 = \lambda_2 w_2 \tag{7}$$

where w is written as a function of λ_1, λ_2 and $1/(\lambda_1\lambda_2)$.

As the present paper only focuses on qualitative results, the Mooney–Rivlin constitutive model is adopted [11,12]. This model is one of the simplest rubber models and it will simplify the following discussion. It is defined by two material constants, C and α, and the corresponding strain energy function is given by:

$$w = C[(\lambda_1^2 + \lambda_2^2 + \lambda_1^{-2}\lambda_2^{-2} - 3) + \alpha(\lambda_1^{-2} + \lambda_2^{-2} + \lambda_1^2\lambda_2^2 - 3)] \tag{8}$$

Using Eqs (7) and (8), the in-plane Cauchy stresses are expressed as:

$$\begin{aligned} \sigma_1 &= 2C\left(\lambda_1^2 - \frac{1}{\lambda_1^2\lambda_2^2}\right)(1 + \alpha\lambda_2^2) \\ \sigma_2 &= 2C\left(\lambda_2^2 - \frac{1}{\lambda_1^2\lambda_2^2}\right)(1 + \alpha\lambda_1^2) \end{aligned} \tag{9}$$

Remark: some results of membrane inflation obtained with more sophisticated constitutive equations are reported by Verron and Marckmann [13].

2.3. Governing equations

The strain energy of the membrane W is obtained by integrating the strain energy function w in the undeformed volume V_0:

$$W = \iiint_{V_0} w dV_0 = \int_0^{l_0} 2\pi w r_0 h_0 ds \tag{10}$$

Let p be the uniform inflating pressure difference across the deformed membrane. Considering that the loading device controls this pressure, the work of the pressure force, T, is the product of the pressure per the volume variation between the deformed and the undeformed configurations:

$$T = p(V - V_0) = \int_0^{l_0} p\pi(r^2 z' - r_0^2 z'_0) ds \tag{11}$$

The total potential energy of the system (membrane and inflating fluid), E, yields:

$$E = W - T \tag{12}$$

Applying the principle of stationary potential energy, the first variation of Eq. (12) must be equal to zero:

$$\delta E = \delta W - \delta T = 0 \tag{13}$$

The first variation of W necessitates the calculation of the variation w. Taking directly into account the incompressibility equation (Eq. (4)), this variation yields to:

$$\delta w = w_1 \delta\lambda_1 + w_2 \delta\lambda_2 \tag{14}$$

So, incorporating stress definition Eq. (7) into Eq. (14), the first variation of the strain energy of the membrane can be written as:

$$\delta W = \int_0^{l_0} 2\pi\left(\frac{\sigma_1}{\lambda_1}\delta\lambda_1 + \frac{\sigma_2}{\lambda_2}\delta\lambda_2\right) r_0 h_0 ds \tag{15}$$

Moreover, after integrating by parts, the first variation of T reduces to:

$$\delta T = \int_0^{l_0} 2p\pi r(z'\delta r - r'\delta z)ds + [\pi p r^2 \delta z]_0^{l_0} \tag{16}$$

In the present paper, only closed membranes are studied, i.e. $r(0) = 0 = r(l_0)$, so the second right hand-side term of Eq. (16) is null.

Finally the principle of stationary potential energy leads to:

$$\int_0^{l_0} 2\pi\left(\frac{\sigma_1}{\lambda_1}\delta\lambda_1 + \frac{\sigma_2}{\lambda_2}\delta\lambda_2\right) r_0 h_0 ds - \int_0^{l_0} 2p\pi r(z'\delta r - r'\delta z)ds = 0 \tag{17}$$

3. Numerical formulations

As shown before, the axisymmetric inflation of hyperelastic membranes involves highly non-linear equations because of large strains and material behaviour. So, a numerical method must be employed to solve the problem. The finite element method is chosen. It consists of discretizing the membrane position and displacement fields, and in deriving the corresponding system of non-linear equations, which must be solved iteratively.

In this section, our finite element approach is presented. As the interpolation method and the resolution scheme were detailed elsewhere [14], the emphasis is laid on the stability analysis of the solution.

3.1. Discretization method and resolution scheme

Note $\mathbf{x}_0(s)$, $\mathbf{u}(s)$ and $\delta\mathbf{u}(s)$ the position, displacement and variation of displacement vectors of a material particle of arc-length co-ordinate s defined by:

$$\mathbf{x_0}(s) = \begin{Bmatrix} r_0(s) \\ z_0(s) \end{Bmatrix} \quad ; \quad \mathbf{u}(s) = \begin{Bmatrix} u_r(s) \\ u_z(s) \end{Bmatrix} \quad ; \quad \delta\mathbf{u}(s) = \begin{Bmatrix} \delta u_r(s) \\ \delta u_z(s) \end{Bmatrix} \tag{18}$$

where $\mathbf{u}_r$ and $\mathbf{u}_z$ are respectively the displacements in the radial and axial directions, and δu_r and δu_z are their corresponding variations.

Consider an isoparametric finite element approximation:

$$\mathbf{x_0}(s) = \mathbf{N}(s)\mathbf{X_0} \quad ; \quad \mathbf{u}(s) = \mathbf{N}(s)\mathbf{U} \quad ; \quad \delta\mathbf{u}(s) = \mathbf{N}(s)\delta\mathbf{U} \tag{19}$$

In these relations, $\mathbf{N}(s)$ stands for the shape function matrix and $\mathbf{X}_0$, $\mathbf{U}$ and $\delta\mathbf{U}$ are the nodal positions, displacements and displacement variations vectors, respectively. Classically, these interpolation formulas are considered in each finite element, said nodal vectors contain the positions or displacements of the nodes of the concerning element. Moreover, in the context of axisymmetric membranes, two nodes finite elements are classically adopted and the shape functions are linear [15,16].

Here, we use a spline interpolation for which every function is interpolated by cubic B-splines. Consequently, nodal vectors contain the parameters of the splines that can be related to more classical nodal variables vectors by constant transform-

ation matrices. Verron and Marckmann extensively studied this spline element [14] and details on B-spline formulations can be found in [17]. One of the major advantages of this interpolation method is its smoothness property. So, the number of nodes necessary to obtain a satisfying solution is highly reduced in comparison with classical finite elements, even for very large strains. Moreover, the tangential boundary condition for nodes that lie on the symmetry axis can be directly incorporated in the model [13].

Noting that the position of a particle in the deformed configuration and its variation counterpart are immediately obtained by:

$$\mathbf{x}(s) = \mathbf{x_0}(s) + \mathbf{u}(s) \quad ; \quad \delta\mathbf{x}(s) = \delta\mathbf{u}(s) \tag{20}$$

and incorporating Eq. (19) into the variational form of the problem (Eq. (17)), the governing equations are reduced to a discrete system of non-linear equations:

$$\mathbf{F_{int}}(\mathbf{U}) - \mathbf{F_{ext}}(\mathbf{U},p) = \mathbf{0} \tag{21}$$

in which the nodal vector of internal forces $\mathbf{F_{int}}$ corresponds to the first left-hand side term in Eq. (17) and only depends on the nodal displacement vector $\mathbf{U}$, and the nodal vector of external forces $\mathbf{F_{ext}}$ corresponds two the second left-hand side term in Eq. (17) and is a function of both the loading pressure p and the displaced configuration $\mathbf{U}$, because the pressure force is a follower force. This system being highly non-linear, it requires an efficient solving algorithm.

Firstly, it has to be noted that loading curves of inflated membranes (in terms of p) exhibit limit points: some parts of the equilibrium path correspond to decreasing pressure values as demonstrated by Beatty [18]. Then, a continuation method is adopted to overcome this difficulty. So, Eq. (21) is augmented with a scalar arc-length equation:

$$|\Delta\mathbf{U}|^2 - da^2 = 0 \tag{22}$$

where $\Delta\mathbf{U}$ stands for the nodal displacement increment between two equilibrium points in the path and da is the prescribed (user-defined) arc-length.

Secondly, the enlarged system Eqs (21) and (22) must be solved by an incremental-iterative scheme, due to non-linearities. Here, we adopt the classical Newton–Raphson algorithm. Consider an equilibrium point defined by $\mathbf{U_e}$ and p_e, the equilibrium nodal displacement vector and inflating pressure. The problem consists in determining the next equilibrium point on the path, i.e. the increments of nodal displacement $\Delta\mathbf{U}$ and pressure Δp that satisfy:

$$\begin{cases} \mathbf{F_{int}}(\mathbf{U_e} + \Delta\mathbf{U}) - \mathbf{F_{ext}}(\mathbf{U_e} + \Delta\mathbf{U}, p_e + \Delta p) = \mathbf{0} \\ |\Delta\mathbf{U}|^2 - da^2 = 0 \end{cases} \tag{23}$$

As the system is solved iteratively, the computation of the tangent operator $\mathbf{\Phi}$ is needed:

$$\mathbf{\Phi} = \begin{bmatrix} \mathbf{K} & -\frac{1}{p}\mathbf{F}_{\mathbf{ext}} \\ 2\Delta\overline{\mathbf{U}} & 0 \end{bmatrix} \tag{24}$$

where $\mathbf{K}$ is the structural tangent matrix of the discretized system, i.e. the derivative of Eq. (21) with respect to $\mathbf{U}$ and $\Delta\overline{\mathbf{U}}$ stands for the previous displacement increment in the iterative scheme.

Note that the previous developments do not refer to the interpolation method adopted and remain valid for every shape function. The explicit formulas of nodal vector forces and tangential operators are proposed by Shi and Moita [19] in the case of the classical linear two-nodes element and by Verron and Marckmann [14] in the case of the spline model.

3.2. Stability and post-critical analysis

As mentioned previously, equilibrium paths of inflated membranes exhibit singular points, i.e. equilibrium points in which the structural behaviour may change suddenly. Two major types of singular points can be defined: limit points in which the slope of the loading curve changes and bifurcation points in which a new equilibrium path occurs. In the previous paragraph, we described the continuation method that is used to overcome limit points. Nevertheless, this method does not permit us to study singular points. In the present paragraph, the stability and post-critical analysis adopted is detailed.

3.2.1. Stability of an equilibrium point

First, before examining the special treatment of singular points, we mention that the stability of an equilibrium point can be simply stated by examining the determinant of the structural tangent matrix $\mathbf{K}$:

- If $\det\mathbf{K} > 0$ then the equilibrium point is stable,
- If $\det\mathbf{K} < 0$ then it is unstable.

3.2.2. Treatment of singular points

Following Seydel [20], the analysis of singular points can be divided in four steps: detecting the occurrence of the singular point, isolating it, determining its nature (limit or bifurcation point) and finally, in the case of a bifurcation point, switching (if desired) onto a secondary branch.

3.2.3. Detection of singular points

In order to detect the occurrence of a singular point, a criterion must be defined. The most natural criterion is the sign change of the determinant of $\mathbf{K}$. But, as shown by Seydel [20], this criterion is not reliable because $\mathbf{K}$ is singular in the neighbour-

hood of a singular point and the computation of its determinant may fail. Shi and Moita [19] adopted the change of the number of negative pivots *INEGP* of **K**. Sokól and Witkowski [21] proposed to calculate a normalised determinant of **K**, $\det_{norm}$, by normalising the determinant with respect to the initial determinant and to consider the following function:

$$f(S) = \begin{cases} +|\det_{norm}| \text{ if } INEGP = m \\ -|\det_{norm}| \text{ if } INEGP \neq m \end{cases} \tag{25}$$

where S can be seen as an arc-length co-ordinate on the equilibrium curve and m stands for the number of negative pivots for the previously computed equilibrium point. Using this function, a singular point corresponds with $f(S) = 0$. In the same paper, authors considered that the most reliable method of detection consists in observing the eigenvalues of **K** but that this method is computer time consuming. Here, due to the spline interpolation that highly reduces the relevant number of degrees of freedom, we calculate explicitly the eigenvalues of **K** and propose the following criterion function g:

$$g(S) = \begin{cases} +\omega_{min} \text{ if } INEG\omega = n \\ -\omega_{min} \text{ if } INEG\omega \neq n \end{cases} \tag{26}$$

where ω_{min} represents the lowest absolute value of the eigenvalues of **K**, $INEG\omega$ is the number of negative eigenvalues of **K** for the present equilibrium state and n stands for this number at the previously computed equilibrium state. Consider an equilibrium state indexed 1 and defined by its arc-length co-ordinate on the path S_1 and its number of negative eigenvalues n_1. Let a second point, indexed 2 and defined by S_2 and n_2, be computed. Then, one or more singular points lie between these two equilibrium points if $g(S_1)g(S_2) < 0$.

3.2.3.1. Isolation of the singular point In order to localise the singular point in the inflating path, we simply use a dichotomy method that consists in determining the previous arc-length co-ordinate S_2 such as $|g(S_2)| < \varepsilon$ where ε is the prescribed precision.

3.2.3.2. Nature of the singular point Consider now that the singular point is isolated, said its position in the path is well known and the corresponding null eigenvalue is identified. Let $\mathbf{Z_{min}}$ denotes the eigenvector associated with this eigenvalue. Then, the nature of the point is simply obtained by examining the scalar product between the eigenvector and the external force [22]:

- If $\mathbf{Z_{min}}.\mathbf{F_{ext}} \neq 0$, this is a limit point,
- If $\mathbf{Z_{min}}.\mathbf{F_{ext}} = 0$, this is a bifurcation point.

3.2.3.3. Branch-switching In the case of a bifurcation point, a secondary branch connected to the primary path occurs at this point. In order to follow this secondary branch, only one new equilibrium point on this branch is needed, and then the calcu-

lation continues on the branch. To switch onto the secondary branch, we adopt the eigen-mode injection method proposed for example by Wagner and Wriggers [23] and successfully used by Shi and Moita [19] for rubberlike membranes. The classical forward Euler predictor is replaced by a prediction in the direction of $\mathbf{Z}_{\mathbf{min}}$:

$$\Delta \mathbf{U}_{\mathbf{prediction}} = da\, \mathbf{z}_{\mathbf{min}} \tag{27}$$

where $\mathbf{z}_{\mathbf{min}}$ is the normalised counterpart of $\mathbf{Z}_{\mathbf{min}}$. The scale factor da is used in order to directly satisfy Eq. (22) in the arc-length method.

4. Results and discussion

4.1. Single balloon

Before examining the case of two connected balloons, the case of a single rubber balloon is recalled. The inflation of a spherical rubber-like membrane was thoroughly studied in the past, both under static [18] and dynamic [24] loading conditions.

Consider a Mooney–Rivlin spherical balloon whose undeformed uniform radius and thickness are respectively R_0 and h_0. As shown by Haughton [25], the balloon remains spherical-shaped during the inflation process. The material parameters are denoted C and α, and the inflating pressure is P. Due to the spherical symmetry, the problem reduces to a one-dimensional equilibrium equation that relates the uniform deformed radius R and the pressure P:

$$P = \frac{4Ch_0}{R_0}\left[\frac{R_0}{R} - \left(\frac{R_0}{R}\right)^7\right]\left[1 + \alpha\left(\frac{R}{R_0}\right)^2\right] \tag{28}$$

Introducing non-dimensional pressure and radius variables, p and λ:

$$p = \frac{PR_0}{4Ch_0} \quad ; \quad \lambda = \frac{R}{R_0} \tag{29}$$

Eq. (28) reduces to:

$$p = \left(\frac{1}{\lambda} - \frac{1}{\lambda^7}\right)(1 + \alpha\lambda^2) \tag{30}$$

where α is the unique relevant parameter.

As shown elsewhere [24], three possible behaviours can be highlighted depending on the values of α: $\alpha = 0.0$, $0.0 < \alpha < \alpha_C$ and $\alpha > \alpha_C$ where α_C is a critical value of the material parameter approximately equal to 0.214. Here, these three behaviours are illustrated by three specific values of α, said 0.0, 0.1 and 0.25. The corresponding inflation curves (non-dimensional pressure versus non-dimensional radius) are presented in Fig. 1.

First, no curve exhibits bifurcation points. As mentioned above, non-spherical deformed configurations never occur for the Mooney–Rivlin strain energy function. In the neo-Hookean case ($\alpha = 0.0$), the path exhibits one limit point that separates

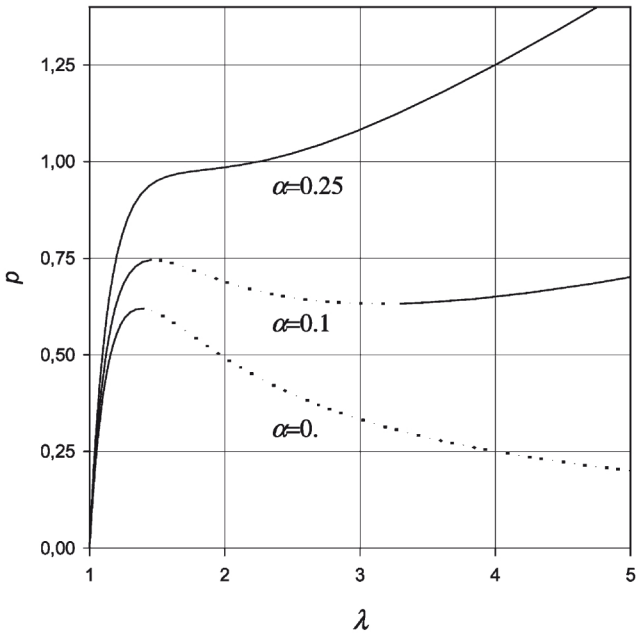

Fig. 1. Inflation of a single spherical balloon for three values of α: (—) stable branches, (···) unstable branches.

one stable branch that corresponds with increasing pressure values and one unstable branch that corresponds with decreasing pressure values. This second branch tends asymptotically to zero as the balloon expands to infinity. For $\alpha = 0.1$, the path admits three branches limited by two limit points. Then, the two stable branches are connected by one unstable branch of decreasing pressure values. Finally, for $\alpha = 0.25$, the pressure always increases as the balloon expands and no limit point exists. Note that in the critical case of $\alpha = \alpha_C$, the two limit points exhibited for $0.0 < \alpha < \alpha_C$ coalesce.

4.2. Two connected balloons

Consider now two identical spherical balloons connected together. Thus, two spheres of initial radius and thickness R_0 and h_0 compose the system, and the internal pressure is equal inside them. Let the material parameter α being equal to 0.1 for both balloons in order to qualitatively describe the phenomenon. In regards with the previous paragraph, such a system may produce remarkable configurations due to the different possible values of the inflating pressure. Fig. 2 illustrates this purpose. In this figure, inflation curves corresponding with the two connected balloons are shown. Non-dimensional radii are denoted λ_I and λ_{II} for the first and the second membranes, respectively. Consider that the balloon I is in the state A defined in the left hand-side plot of Fig. 2. The balloon II can afford three different configurations

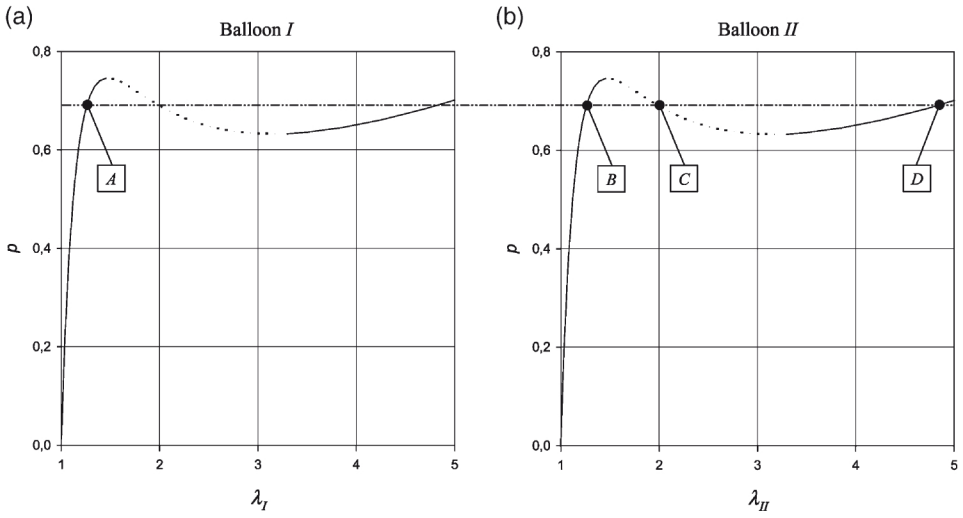

Fig. 2. Possible equilibria of two connected balloons: (a) balloon *I*, (b) balloon *II*; (—) stable branches, (···) unstable branches.

B, *C* and *D*, as shown in the right hand-side plot of Fig. 2. Therefore, it becomes obvious that the inflation curve of the present system is highly different from the inflation curve of a unique sphere: there are different equilibrium paths and then some bifurcation points for the global system.

In order to establish the inflation paths, we consider the system of two connected spheres meshed with 39 nodes. For numerical convenience, the undeformed radii of both spheres are set to 1.0, and the initial thickness is 0.01. As mentioned above, only non-dimensional variables λ_I, λ_{II} and p are considered, and the only relevant parameter is α. The interpolated membranes are presented in Fig. 3. The following boundary conditions are adopted: the middle node is fixed and both extreme nodes must remain in the symmetry axis. The three different values of α considered in the previous paragraph are examined. In each case, two branching diagrams will be drawn: the first one (indexed (a)) is the 2D plot that shows the possible equilibrium points in the (λ_I, λ_{II})-diagram and the second one (indexed (b)) is the 3D plot where equilibrium states are drawn into the (λ_I, λ_{II}, p)-diagram.

Let first examine the case of the neo-Hookean material, i.e. $\alpha = 0.0$. The corresponding branching diagrams are presented in Fig. 4. At the beginning of the inflation process, the two balloons inflate similarly until they reach the point a_0 in the branching diagrams 4(a) and (b). This first part of the path is obviously stable and corresponds to the stable increasing pressure branch previously observed for a single balloon in Fig. 1. For the single balloon, the state a_0 is a limit point. In the present case, two singular points coincide in a_0: a limit point that corresponds to the change of pressure slope and a bifurcating point that defines the possibility to switch onto secondary branches where $\lambda_I \neq \lambda_{II}$. Numerically, the position of the two coincident singular points is isolated and the two corresponding eigenvectors are computed in

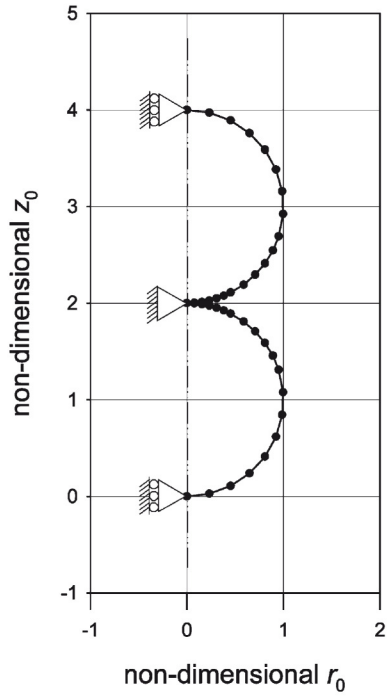

Fig. 3. Interpolated membrane used for simulations.

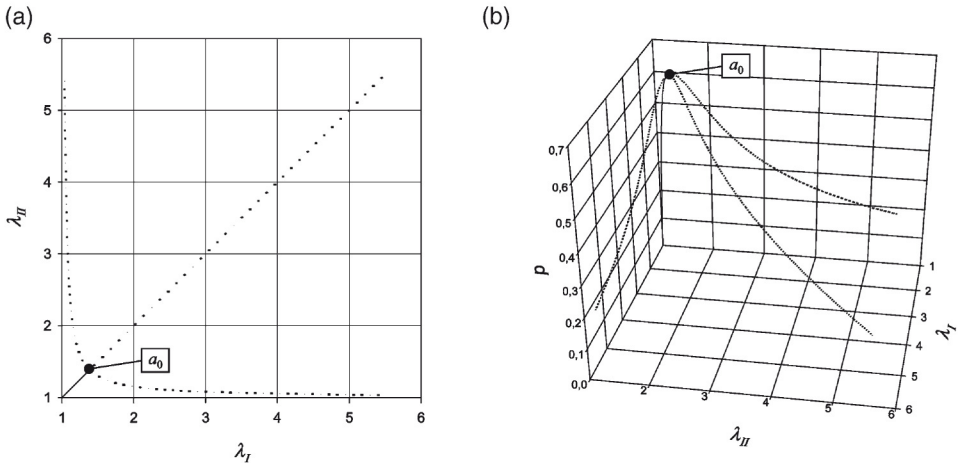

Fig. 4. Equilibrium diagrams for $\alpha = 0$: (a) 2D representation, (b) 3D representation; (—) stable branches, (···) unstable branches.

order to determine their respective natures. Then, for the bifurcating point, it is possible to switch onto a secondary branch. Here, the primary path is the branch where the two radii remains equal, this path is easily explored without switching. The secondary paths are the two asymmetric paths in which one of the balloon expands as the other reduces and finally disappears, i.e. one radius tends to infinity and the other one tends asymptotically to zero as the total volume of fluid in the system increases. These secondary paths are also unstable. Note that the numerical method furnishes only one of the two asymmetric branches, the other one can be computed by changing the sign of the corresponding eigenvector for the prediction in the branch-switching algorithm (see Section 3). Finally, we have to determine if the balloon follows the symmetric or the asymmetric path when the fluid is continuously injected inside the system, i.e. what is the more "stable" of these two unstable configurations? The simplest method to answer this question consists in adding an initial default in the structure and in examining which branch the system follows. Thus, a new simulation is performed assuming that the initial radius of the balloon *II* is equal to 1.001. It is observed that the system follows the asymmetric path in which the balloon *I* inflates the balloon *II* and tends to disappear as the total volume of fluid increases. These results are similar to those derived analytically by Weinhaus and Barker [4] with the same constitutive equation, and by Read [5] that uses the generalised Hooke's law for finite strains.

Consider now the more interesting case in which $\alpha = 0.1$. The corresponding diagrams are presented in Fig. 5. As shown previously, the single balloon inflation curve has two stable branches, one at small strains and one at large strains. That is the reason why the equilibrium 2D map in Fig. 5(a) exhibits two solid lines (stable paths) with $\lambda_I = \lambda_{II}$. The first one is located between the initial unloaded state and the first singular point a_1, that corresponds to the first limit point of the $\alpha = 0.1$ curve in Fig. 1. It represents the behaviour of the system at relatively small strains,

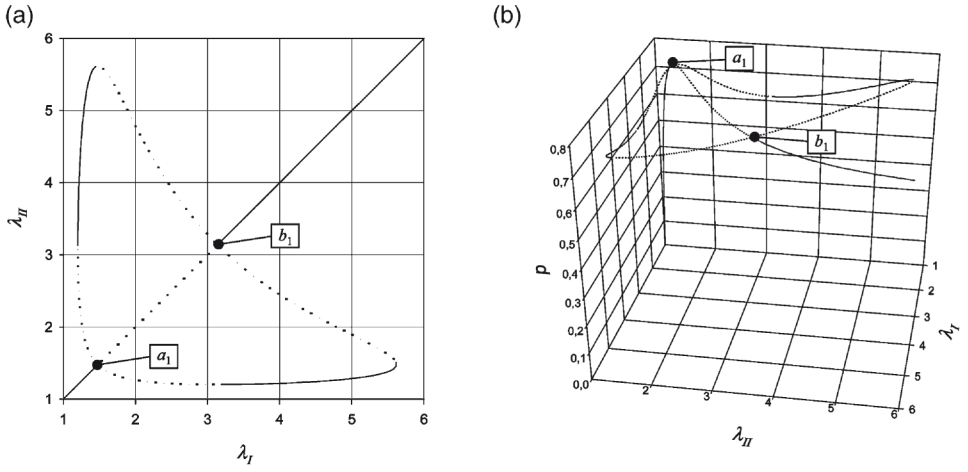

Fig. 5. Equilibrium diagrams for $\alpha = 0.1$: (a) 2D representation, (b) 3D representation; (—) stable branches, (···) unstable branches.

i.e. for a small amount of fluid inside the system. The second stable branch goes from the point b_1 (the second limit point of the $\alpha = 0.1$ curve in Fig. 1) to infinity and defines the behaviour of the balloons under large strains, i.e. for a large amount of fluid in the system. These two parts of the equilibrium diagram are obviously stable because they correspond to ascending pressure situations (see Fig. 5(b)). Points a_1 and b_1 are detected and isolated during the simulation. They have the same status as the point a_0 described in the previous paragraph: two different singular points (one limit point and one bifurcating point) coincide at them. Using the switching procedure, it is possible to explore secondary paths. First, the symmetric dotted path ($\lambda_I = \lambda_{II}$) between a_1 and b_1 is the primary path: it is obtained without switching in a_1. Then, as the amount of fluid increases, the two balloons inflate similarly and follow the loading curve of the single balloon (Fig. 1), said two stable branches and one unstable branch. Second, if the switching procedure is activated in a_1, one of the two asymmetric branches is followed, said for example $\lambda_I < \lambda_{II}$. Then, as the simulation continues, the system follows the entire closed loop passing through b_1 and it ever remains on the loop. It does not find the symmetric path again. Moreover, it is easily shown that the asymmetric path is more stable than the symmetric one using an imperfect system. The present results are in agreement with the results obtained analytically by Dreyer et al. [6] and Müller [7]. The only difference concerns the stability status of the closed loop: here, we show that two parts of it (the parts with decreasing pressure values) are unstable when only one part of it was said to be unstable in the cited references.

Finally, the case $\alpha = 0.25$ is obvious. It was shown in Section 4.1 that the pressure inside a single balloon always increases as it expands and that the equilibrium curve is always stable. Thus, the system of two balloons remains stable whatever the amount of fluid inside it and the branching diagram is reduced to one path of equal radii, as shown in Fig. 6(a) and (b). Both membranes follow the path of the single balloon shown in Fig. 1.

5. Concluding remarks

In this paper, the problem of the inflation of connected rubber balloons is solved using both a finite element analysis and a bifurcating procedure for singular points. The influence of material parameters, especially one of the two Mooney–Rivlin constants, on the response of the system is demonstrated and thermodynamical results proposed in the bibliography are recovered.

The present work leaves some issues of importance unanswered. One of these is the use of more complex hyperelastic constitutive equations, such as the Ogden's model [10], for the modeling of the rubber behaviour. It was shown by Haughton [25] that an Ogden single balloon exhibits bifurcating non-spherical states. This phenomenon was confirmed experimentally by Alexander [26]. So, the behaviour of two connected spheres will be more complicated than in the present case; and the branching diagrams will exhibit more bifurcating branches. This problem will be examined in further works.

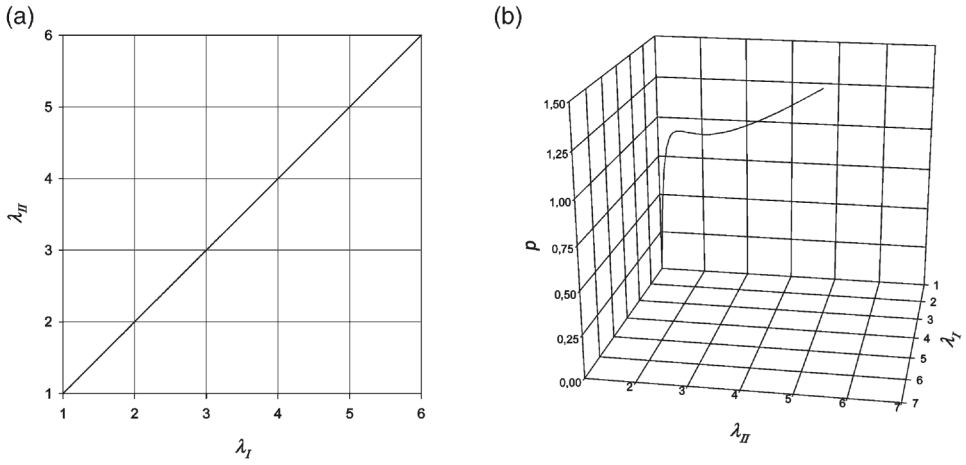

Fig. 6. Equilibrium diagrams for $\alpha = 0.25$: (a) 2D representation, (b) 3D representation; (—) stable branches, (···) unstable branches.

References

[1] Miller JS. Pressure within a bubble. American Journal of Physics 1952;20:115.
[2] Boys CV. Soap bubbles—their colours and forces which mold them. New York: Dover, 1959.
[3] Isenberg C. The science of soap films and soap bubbles. Clevendon: Tieto, 1978.
[4] Weinhaus F, Barker W. On the equilibrium states of interconnected bubbles or balloons. American Journal of Physics 1978;46:978–82.
[5] Read G. An application of elementary calculus to balloons. European Journal of Physics 1986;7:236–41.
[6] Dreyer W, Müller I, Strehlow P. A study of equilibria of interconnected balloons. Quarterly Journal of Mechanics and Applied Mathematics 1982;35:419–40.
[7] Müller I. Two instructive instabilities in non-linear elasticity: biaxially loaded membrane, and rubber balloons. Meccanica 1996;31:387–95.
[8] Green AE, Adkins JE. Large elastic deformations. Oxford, UK: Clarendon Press, 1960.
[9] Khayat RE, Derdouri A, Garcia-Réjon A. Inflation of an elastic cylindrical membrane: non-linear deformation and instability. International Journal of Solids and Structures 1992;29:69–87.
[10] Ogden RW. Nonlinear elastic deformations. New York: John Wiley & Sons, 1984.
[11] Mooney M. A theory of large elastic deformation. Journal of Applied Physics 1940;11:582–92.
[12] Treloar LRG. The mechanics of rubber elasticity. Proceedings of the Royal Society of London 1976;A351:301–30.
[13] Verron E, Marckmann G. Inflation of elastomeric circular membranes using network constitutive equations. International Journal of Non-linear Mechanics 2003;38:1221–35.
[14] Verron E, Marckmann G. An axisymmetric B-spline model for the non-linear inflation of rubberlike membranes. Computer Methods in Applied Mechanics and Engineering 2001;190:6271–89.
[15] Charrier JM, Shrivastava S, Wu R. Free and constrained inflation of elastic membranes in relation to thermoforming-axisymmetric problems. Journal of Strain Analysis 1987;22:115–25.
[16] Hassager O, Kristensen SB, Larsen JR, Neergaard J. Inflation and instability of a polymeric membrane. Journal of Non-Newtonian Fluid Mechanics 1999;88:185–204.
[17] De Boor C. A practical guide to spline. New York: Springer-Verlag, 1978.
[18] Beatty MF. Topics in finite elasticity: hyperelasticity of rubber, elastomers, and biological tissues—with examples. Applied Mechanics Reviews 1987;40:1699–734.

[19] Shi J, Moita GF. The post-critical analysis of axisymmetric hyper-elastic membranes by the finite element method. Computer Methods in Applied Mechanics and Engineering 1996;135:265–81.
[20] Seydel R. Practical bifurcation and stability analysis. New York: Springer-Verlag, 1994.
[21] Sokól T, Witkowski M. Some experiences in the equilibrium path determination. Computer Assisted Mechanical Engineering Science 1997;4:189–208.
[22] Spence A, Jepson AD. Folds in the solution of two parameter systems and their calculation. Part I. SIAM Journal of Numerical Analysis 1985;22:347–68.
[23] Wagner W, Wriggers P. A simple method for the calculation of postcritical branches. Engineering Computation 1988;5:103–9.
[24] Verron E, Khayat RE, Derdouri A, Peseux B. Dynamic inflation of hyperelastic spherical membranes. Journal of Rheology 1999;43:1083–97.
[25] Haughton DM. Post-bifurcation of perfect and imperfect spherical elastic membranes. International Journal of Solids and Structures 1980;16:1123–33.
[26] Alexander H. Tensile instability of initially spherical balloons. International Journal of Engineering Science 1971;9:151–62.